# Surface characterization of nanoporous aluminium oxide films synthesized by single-step DC and AC anodization

**Article** *in* Tribology - Materials Surfaces & Interfaces · June 2017

DOI: 10.1016/j.surfin.2017.04.001

CITATIONS
7

READS
523

**5 authors**, including:

Nagaraj Chelliah Machavallavan
PSG College of Technology
**15** PUBLICATIONS **142** CITATIONS
SEE PROFILE

Alaukik Saxena
Interdisciplinary Centre for Advanced Materials Simulation
**1** PUBLICATION **7** CITATIONS
SEE PROFILE

Harpreet Singh
Indian Institute of Technology Ropar
**231** PUBLICATIONS **3,123** CITATIONS
SEE PROFILE

Mirle Surappa
Indian Institute of Technology Ropar
**101** PUBLICATIONS **4,093** CITATIONS
SEE PROFILE

Surfaces and Interfaces 7 (2017) 139–145

Contents lists available at ScienceDirect

Surfaces and Interfaces

journal homepage: www.elsevier.com/locate/surfin

# Surface characterization of nanoporous aluminium oxide films synthesized by single-step DC and AC anodization

Nagaraj M. Chelliah[a], Alaukik Saxena[a], Khushdeep Sharma[a,b], Harpreet Singh[a,*], M.K. Surappa[c]

[a] Department of Mechanical Engineering, Indian Institute of Technology Ropar, Rupnagar 140001, Punjab, India
[b] Department of Advanced and Materials Processing, Friedrich-Alexander-Universitat Erlangen, Nurnberg 91054, Germany
[c] Department of Materials Engineering, Indian Institute of Science, Bengaluru 560012, Karnataka, India

ARTICLE INFO

*Keywords:*
Anodization
Aluminum oxide
Fast Fourier transform
Surface morphology
Atomic force microscopy (AFM)

ABSTRACT

Nanoporous alumina films were synthesized on commercial grade aluminum substrates using single-step anodization technique in 0.3 M phosphoric acid at room temperature. Effect of applied voltage (100–130 V) on surface characteristics of anodized aluminum oxide (AAO) film was investigated. Surface topography parameters and regularity ratio of nanopores arrangement were characterized using power spectral density (PSD) and fast Fourier transform (FFT) profiles. While DC anodization suffered from filament-like cavities at 130 V owing to thermally enhanced dissolution of oxide, AC anodization produced localized flower-like morphology for all the applied voltages. The intensity of localized flower-like morphology was increased monotonically with applied voltage. Evolution of flower-like morphology was discussed on the basis of Pashchanka-Schneider model.

## 1. Introduction

Nanoporous anodic aluminum oxide (AAO) has a tremendous potential in large spectrum of nano-scale engineering applications ranging from template-assisted synthesis of nanowires to MEMS/NEMS based tribology devices [1–4]. Numerous efforts have been made in the literature to understand the mechanism of pattern formation during aluminum anodization [5–10]. The field-assisted dissolution model [5–9] suggests that oxide film growth occurs at the metal/oxide interface owing to inward migration of $O^{2-}$ ions across the barrier layer and the pores are formed mainly at the oxide/electrolyte interface due to electric field-accelerated dissolution of anodic alumina accompanied by outward migration of $Al^{3+}$ ions into the electrolyte. The stress-driven viscous flow model [10–12] claims that nanopores are generated mainly by flow of material from the pore bases to the cell walls and this material displacement is primarily facilitated by plasticity of the oxide film. The oxygen bubble model [13–15] emphasizes that the evolution of $O_2$ occurs with the formation of oxide film, and whether or not this oxide film has been transformed from barrier type to porous type, can be determined by observing whether or not $O_2$ separates out of the bulk oxide film. Later, Pashchanka et al [16–18] proposed the novel theoretical model for nanoporous pattern formation by adopting the analogy of Rayleigh-Bernard convection cells. While the temperature gradient is the driving for Rayleigh-Bernard convection cells, the applied voltage is considered as a driving force for pattern formation in porous oxide film [16]. However, it is very difficult to provide the unified theory describing all the aspects of random experimental observations during aluminum anodization. Nevertheless, Pashchanka-Schneider model describes the wide range of unexplained experimental observations for the formation of equal-sized hexagonally ordered pores [16].

The self-ordering of nanopores in anodized aluminium oxide (AAO) film is governed by several anodization parameters such as applied voltage [19], time [20], temperatures [20] and pH [21], concentration [21], conductivity, viscosity [22] and composition [23] of the applied electrolyte. Pashchanka et al [16] proposed an empirical relationship between these anodization parameters as follows:

$$P = \frac{Q_{av}\Delta U}{\eta} = \frac{10^{-pH}\Delta U}{C\eta} \quad (1)$$

Where P is the porosity number or criterion for the appearance of self-organized nanopores (found experimentally to be around 0.057 for the majority of the widely used electrolytes), $Q_{av}$ is the average charge of supporting electrolyte anions, $10^{-pH}$ is the proton concentration, $\Delta U$ is the applied voltage, η is the dynamic viscosity, σ is the specific electrical conductivity and $C$ is the acid concentration. The Eq. (1) demonstrates that the self-ordering voltage mainly depends upon the applied electrolyte. For instance, the lower voltages (15–30 V) are preferred for the less viscous solutions of sulfuric acid and oxalic acid while the higher voltages (160–195 V) for a viscous phosphoric acid

* Corresponding author at: School of Mechanical, Materials and Energy Engineering, 208 SMMEE, Rupnagar, 140001, India.
*E-mail addresses:* harpreetsingh@iitrpr.ac.in, hnr97@yahoo.com (H. Singh).

http://dx.doi.org/10.1016/j.surfin.2017.04.001
Received 16 November 2016; Received in revised form 12 March 2017; Accepted 3 April 2017
Available online 04 April 2017

[16]. Stepniowski et al [20] investigated the influence of time and temperature on the arrangement of alumina nanopores. They observed that the better ordering of alumina nanopores occurs in second-step anodization if first-step anodization is performed for longer duration owing to better pre-texturing of the aluminum beneath the pore bottoms, at the metal–oxide interface and the applied temperature has no effect on ordering of nanopores for a short time anodization. Stepniowski et al [21] mentioned that interpore distance between nanopores linearly scales with applied voltage while it increases exponentially with molar fraction of chromic acid electrolyte.

Most researchers synthesized self-organized nanoporous aluminum oxide films by utilizing the combination of high purity aluminum substrate and low temperatures (0-10 °C) by using DC anodization [24–27]. This combination is generally preferred as the existence of any chemical impurities shall not allow sustainable growth of oxide film owing to thermally enhanced dissolution and dielectric breakdown [28] at the metal-oxide interface during DC anodization. However, there has been significant interest among the aluminum industry for alternating current (AC) and pulsed current anodization to fabricate nanoporous AAO films on commercial grade Al-alloys and low purity aluminum substrates under ambient environment [29–33]. De Graeve et al [29] investigated the contribution of cathodic process during AC anodization of commercial Al-alloys, and observed that cathodic hydrogen gas evolution develops high cathodic potential at flaw sites tending to reduce the efficiency of film formation. In recent years, pulsed current techniques seem to be gaining attraction since it overcomes most of the disadvantages (thermally enhanced dissolution of DC anodized film, limited thickness, and inferiority in the quality of AC anodized film) associated with conventional DC and AC anodization techniques. Lee et al [31] proposed pulse anodization approach that combines the advantages of mild anodization (formation of self-ordered nanopores) and hard anodization (high production rate). Law et al [32] tailored the optical properties of AAO photonic crystals by controlling the various anodization parameters precisely using sawtooth-like pulse anodization. Chung et al [33,34] proposed the novel hybrid pulse anodization technique to synthesize AAO films on commercial grade purity Al substrates (99%) at room temperature condition itself. The basic idea behind this hybrid pulse approach was to suppress any temperature rise by facilitating the cooling of electrolyte during the pulse-off period. The incorporation of cathodic cycle using alternating current may reduce the dissolution tendency of oxide layer at impurity sites to the certain extent. It is noted that certain engineering applications such as hydrogen gas storage [35,36], catalysis [37,38], electrochemical sensing [39] , membrane synthesis [40,41] and corrosion protection coatings [21,42,43] shall not need any self-organized or well-ordered nanopores. Moreover, AC anodization has distinct practical advantages relative to DC anodization. For instance, it is possible to obtain anodization for two different aluminum substrates at the same time during AC anodization. AC anodization also minimizes the necessity for pretreatment of the aluminum substrates and agitation of anodizing electrolyte owing to hydrogen gas evolution during cathodic cycle. In fact, AC anodization can be considered as one of the simplest, economic and affordable industrial techniques in the mass production of corrosion protection coatings for large-scale aluminum sheet and food packaging applications [29]. Despite the mechanism of nanoporous oxide formation during AC anodization is similar to that of DC anodization; the characteristics of film morphology, surface topography and regularity ratio of poorly arranged nanopores may be varied as a function of applied voltage during AC and DC anodization. Furthermore, the nature of film morphology and surface topography play decisive role in determining the mechanical and frictional behavior of AAO films for surface engineering related applications [44–46]. Main objective of the present study was to understand the evolution of film morphology, surface topography and regularity ratio of poorly arranged alumina nanopores obtained on commercial grade Al substrates by varying applied voltage (100–130 V) using single-step DC and AC anodization.

## 2. Experimental methods

Commercial grade Al substrates of 99.0% purity were utilized to fabricate nanoporous aluminium oxide films by single-step anodization. Firstly, the surface area of Al specimens (15 mm x 15 mm x 0.25 mm) was coated with an insulative polymer film after leaving an exposed area of 1 $cm^2$ for anodization process. Al specimens were then subjected to chemical polishing in 1 M solution of NaOH for two min in order to achieve the mirror-like surface finish. Subsequently, single-step D.C. and A.C. anodization were performed on these polished Al substrates in 0.3 M phosphoric acid solution at a constant applied voltage of 100, 110, 120 and 130 V for 15 min. DC-current was supplied from DC power source (Zeal-Tech instrument, Model No.9211, India) while AC-current was supplied from single phase auto transformer (Crown Instrument, Model No.C10ASPT, India). All the anodization experiments were performed at room temperature (30–35 °C) and water bath was used as a heat sinking source during anodization. The presence of thin whitish gray layer on Al substrates confirmed the formation of AAO films. Three specimens were prepared for each set of process parameters to ensure repeatability in the experimental data. It should be kept in mind that single-step anodization results in the formation of poorly arranged nanopores, unlike two-step anodization which leads to the formation of well-ordered hexagonal nanopores. Surface characteristics of AAO films fabricated on commercial grade aluminum substrates were analyzed by scanning electron microscope (SEM, JEOL JSM-6610LV, Japan), and atomic force microscope (AFM, Bruker Multimode 8, USA) respectively. Power spectral density (PSD) and Fast Fourier transforms (FFT) profiles were derived from AFM images and SEM micrographs in order to evaluate the surface topography parameters and regularity ratio of pore arrangement for all the AAO films, synthesized at various D.C. and A.C. voltages.

## 3. Results and discussion

Fig. 1 depicts the variation of current as a function of time for both AC and DC anodization. In typical AC anodization, the aluminum specimen serves as an anode for every 0.01 s (at a given frequency of 50 Hz) and for the same consecutive period, it acts as a cathode due to polarity shift in the voltage. However, aluminum remains as anodic material during the entire period for the case of DC anodization. Fig. 2 shows the SEM micrographs which represent the evolution of surface morphology of anodized specimens performed by DC and AC anodization techniques. It is evident that the nature of surface morphology is more or less appeared to be similar at 100 V (compare Fig. 2(a) and

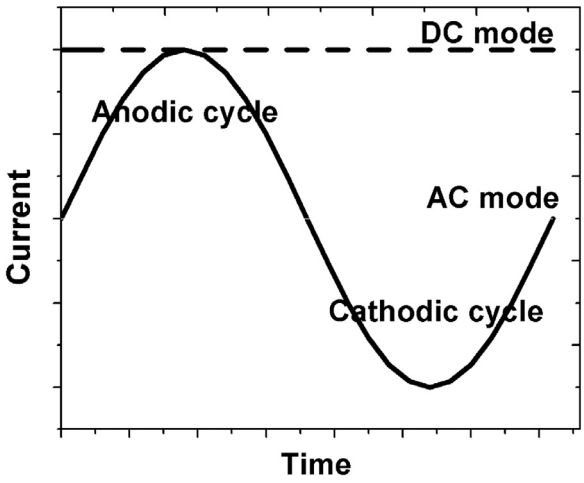


**Fig. 1.** Variation of current as a function of time for DC and AC anodization process.

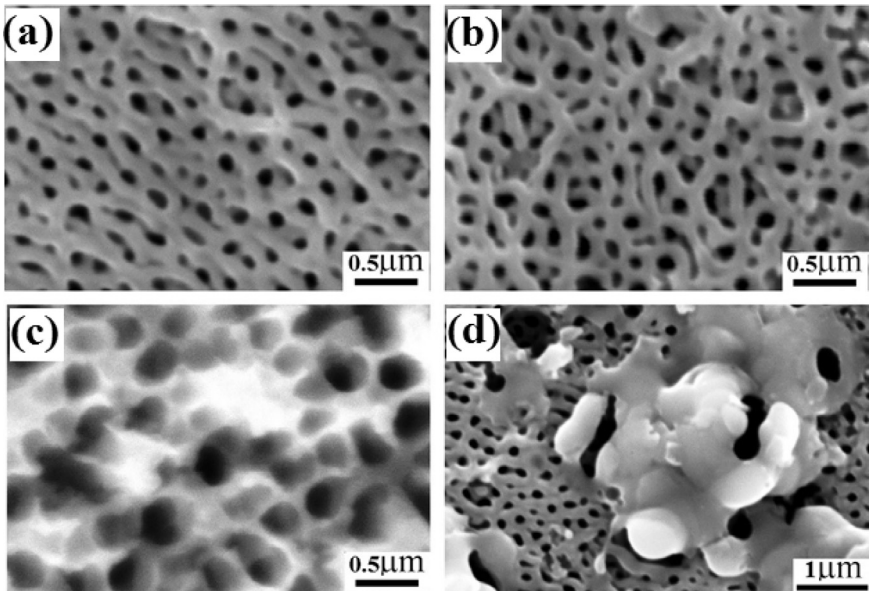


**Fig. 2.** Surface morphologies of anodized commercial grade aluminum specimens, (a) & (b) DC & AC anodization performed at 100 V; (c) & (d) DC & AC anodization performed at 130 V respectively.

(b)). On the contrary, the filament-like cavities are observed for DC anodized specimen at 130 V as seen in Fig. 2(c). The existence of filament-like cavities could be associated with the thermally enhanced dissolution of oxide film. When impurities accommodated within commercial grade aluminum are subjected to high electrical resistivity, it causes sudden temperature rise of an electrolyte which eventually leading to induce thermally enhanced dissolution of oxide at the electrolyte/anode interface [32] . It is well-known fact that Joule's heat linearly scales with an applied voltage during anodization. Therefore, when applied voltage approaches 130 V, anodized specimen may experience the maximum Joule's heat within the electrolyte. This demonstrates that DC mode exhibits thermally enhanced dissolution of oxide film at impurity sites after certain amount of Joule's heat is achieved and this happens only at 130 V. However, there is no evidence of thermally enhanced dissolution of oxide film for the case of AC anodization at any applied voltage in the present work. It is believed that the introduction of cathodic cycle may suppress the abrupt rise in Joule's heat within the electrolytic medium. Most importantly, it can be seen that AC anodization represents the evolution of localized flower-like morphology over the anodized surface at 130 V (Fig. 2(d)). The summary of important geometrical parameters which were quantified after anodization is provided in Table 1. The measured pore diameters of nanopores for AC as well as DC anodization from SEM micrographs are found to be in the range of 90–100 nm except the specimen anodized at 130 V during DC anodization (Table 1). The existence of higher pore diameter (278 nm) for DC anodization performed at 130 V can be ascribed to the thermally enhanced dissolution owing to higher amount of Joule's heat.

Fig. 3 depicts the low-resolution SEM images of nanoporous structures of AAO films obtained using AC anodization under different voltages. It can be seen that the intensity of localized flower-like morphology increases monotonically with increasing applied voltage. At this moment, it is worthwhile to understand the mechanism of nanoporous oxide formation in accordance with Pashchanka-Schneider model [16] during DC anodization as follows; Firstly, hydrated anions are attracted towards aluminium during anodic cycle. These hydrated anions have a shell of water molecules around them. Aluminium reacts with water molecules to form colloidal alumina particles along with generation of protons which tends to lower the pH locally near the aluminium surface according to the following equation [16];

$$Al + 2H_2O \rightarrow Al\ (O)OH\ (boehmite) + \ 3H^+ + 3\ e^- \quad (2)$$

These colloidal alumina particles cannot precipitate directly on aluminium substrate owing to low pH. However, at a certain distance away from the working electrode, pH is locally increased because of the attracted $OH^-$ ions from the electrolyte [16]. The negative charge is accumulated near the anode due to the migration of hydrated anions towards the aluminum surface [16]. Each new migrating hydrated anion experiences the repulsion forces from the accumulated charge along with the attraction by the electromagnetic force [16].

Once the critical concentration gradient of hydrated anions is attained, they start to move in the opposite direction due to the conventional diffusion process [16]. This diffusion decreases the accumulation of negative charge near the anode and facilities the delivery of newly hydrated anions to participate in the chemical reaction as mentioned in the Eq. (2). The competition between two driving forces (electromagnetic attraction and diffusion of hydrated anions) creates concentration and current fluctuations. This scenario activates steady-state exchange of anions and ionic currents akin to convective currents for Rayleigh-Bernard cells [16].

By steady-state exchange of anions, the mobile colloidal alumina particles are escaped away from the aluminum surface and migrate to the region where there exists a scarcity of $H^+$ ions and get neutralized with $OH^-$ ions attracted from the electrolyte [16]. On this region, pH increases locally. Therefore, these colloidal alumina particles can now be able to coagulate and precipitate above the aluminum substrate in order to form an inter-pore wall [16]. Once the inter-pore wall is formed, it is lifted up by the newly colloidal particles from below and leading to the formation of nanoporous pattern [16]. According to Pashchanka-Schneider model [16], the applied voltage should be around 160 V to obtain any self-ordering of alumina nanopores in

**Table 1**
Summary of important geometrical parameters for DC and AC anodized films.

| Voltage | Pore diameter, nm | | RMS roughness, nm | | Average regularity ratio | |
|---|---|---|---|---|---|---|
| | DC | AC | DC | AC | DC | AC |
| 100 | 94 | 91 | 44 | 29 | 1.8 | 2.9 |
| 110 | 99 | 110 | 43 | 47 | 2.5 | 4.4 |
| 120 | 105 | 89 | 43 | 48 | 2.7 | 4.9 |
| 130 | 278 | 95 | 152 | 79 | 1.1 | 5.9 |

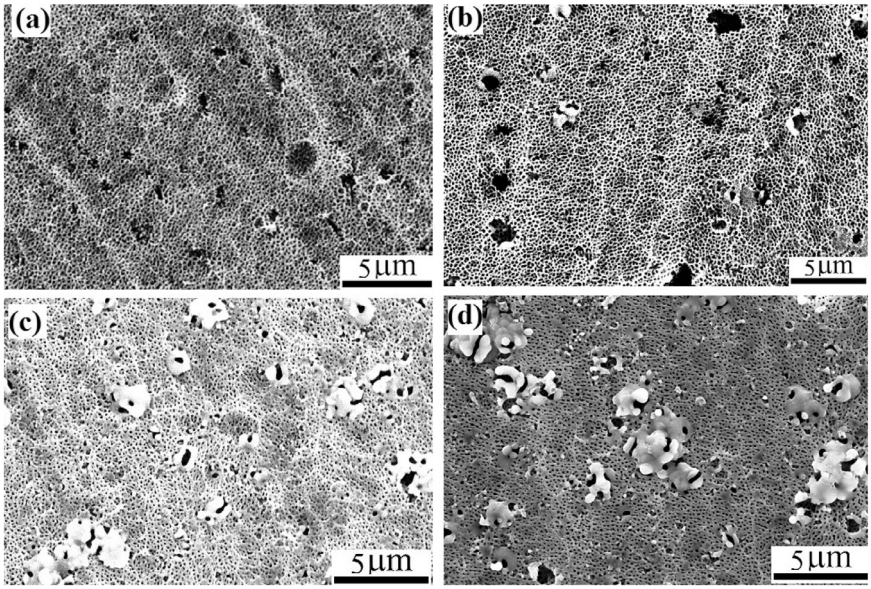


**Fig. 3.** SEM micrographs of anodized commercial grade aluminum samples performed by AC anodization at different voltages (a) 100 V, (b) 110 V, (c) 120 V, and (d) 130 V.

phosphoric acid electrolyte. Most of the experimental observations also suggest that self-ordering voltage should be in the range of 160–195 V for the case of 0.3 M phosphoric acid [16]. Since the range of applied voltage in the present work lies between 100–130 V, the self-ordering of alumina nanopores has not been expected. In fact, SEM examination confirms that alumina nanopores are not well-organized or poorly arranged irrespective of the applied voltage during AC anodization as well as DC anodization.

Fig. 4 illustrates the schematic model for the formation of flower-like morphology on the basis of Pashchanka-Schneider model [16]. Despite this model is mainly suggested for DC anodization, it can be utilized to explain how localized flower-like morphology emerges over the free surface of AAO film during AC anodization. Firstly, the mechanism of inter-pore wall generation is caused by the steady-state exchange of the ions during anodic cycle of AC anodization as described in Pashchanka-Schneider model. Later, the porous oxide formation is

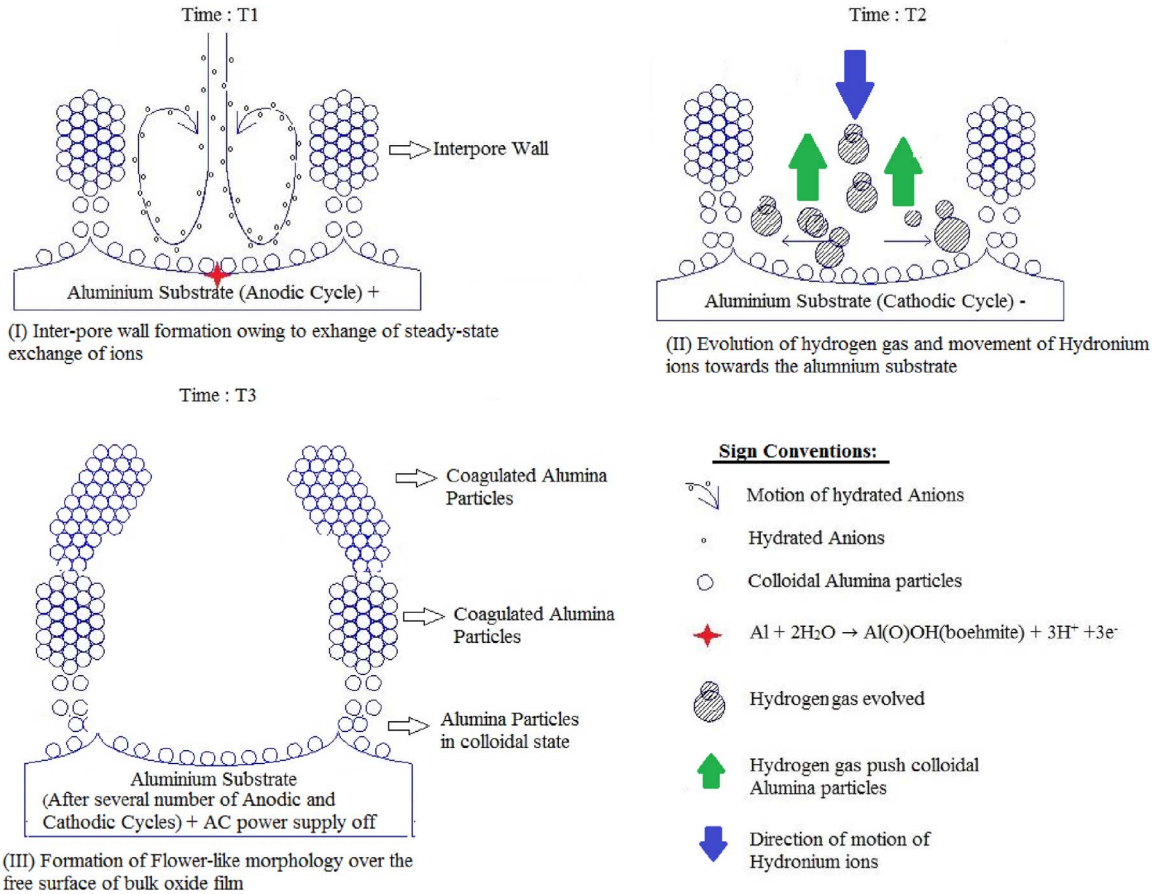


**Fig. 4.** A schematic mode illustrates the formation of flower-like morphology during AC Anodization in accordance with Pashchanka-Schneider model [16].

hindered due to shift in polarity by the introduction of cathodic cycle during AC anodization. In the mean time, there is an evolution of hydrogen gas at preferential sites having majority of flaws or impurities [5]. Furthermore, attractions of hydronium ions towards the cathode tending to lower the pH locally near the aluminium substrate. Therefore, the alumina particles those were produced during previous anodic cycle did not get a chance to coagulate and remain to be in the colloidal state. This evolving hydrogen gas pushes away these mobile colloidal alumina particles out of the bulk oxide film. After several numbers of anodic and cathodic cycles, those alumina particles which were pushed outside of the bulk porous oxide film are still in the colloidal state owing to low pH in the remote electrolyte. Once, we turn off the AC power supply, the production of both $H^+$ and hydrogen gas stops and pH is raised locally in this surface region. This favors the settling of colloidal alumina particles which eventually results in the emergence of flower-like morphology over the free surface of the bulk porous oxide film. It should be noted that the magnitude of pushing, and settling of these colloidal alumina particles dictate the intensity of flower-like morphology. The trend in the intensity of localized flower-like morphology demonstrates that the magnitude of pushing and settling of colloidal alumina particles increases with increasing of applied voltage. This may be ascribed to the evolution of larger amount of hydrogen gas during AC anodization.

3D AFM images contrast the difference in surface roughness between DC and AC mode anodized at similar applied voltage of 130 V (compare Fig. 5(a) and (b)). Fig. 5(c) depicts the variation of (RMS, root mean square) roughness as a function of applied voltage for both DC and AC anodization. It can be seen that RMS roughness values remain constant until 120 V and reached its maximum value at 130 V during DC anodization, whereas roughness values vary moderately for the case of AC anodization. This abrupt increase in RMS roughness value can be associated with thermally enhanced dissolution. It is pertinent to mention that RMS roughness values do not truly represent the exact surface topographic variations that existed in anodized samples as roughness parameter is highly sensitive to the length scale of measurement; hence we preferred to obtain power spectral density (PSD) profile by using atomic force microscopic technique [47]. Fig 6(a) and (b) show the power spectral density spectra of anodized samples performed at DC and AC mode for different voltages. It is well-documented that the slope of high-frequency domain refers to local roughness or fractal components, and power intensity at low-frequency domain gives the information related to the strength of the aggregates or global roughness. On the high-frequency domain, it can be observed that local roughness increases slightly with the applied voltage for the case of AC anodization. However, roughness remains almost constant in DC anodized specimen except at 130 V where thermally enhanced dissolution accelerates. The directional flow of ions remains constant during DC anodization where one can expect the constant roughness profile for DC anodized specimen. However, the uni-directional flow of ions is often changed or interrupted for the case of AC anodization owing to shift in the polarity for every 0.01 s.

Fig. 7 represents typical radial averages of fast Fourier transform (FFT) profiles obtained from SEM images of DC and AC anodized specimen. The radial average of FFT profiles of alumina nanopores were obtained by using a methodology adopted by Wojciech et al [48] . FFT profile was generated from SEM micrographs using WSxM software [49,50]. It is noted that physical meaning of radial average is nothing but a distribution of interpore distance in the inversed space. The intensity of FFT profile refers to the regularity of pore arrangement and FFT radius measures the average inter-pore distance. The width of full intensity at half of its height can be related to uniformity in the distribution of low-ordered nanopores. Regularity ratio of nanoporous arrangement within alumina films can be estimated from the radial average of FFT profile according to the following equation;

$$R = \frac{\sqrt{n}\ H}{S^{3/2}W} \tag{3}$$

where: n is number of pores, H is the maximum intensity of the FFT radial average, S is analyzed surface area and width of the radial average at half of the maximum intensity from FFT profile. The lowest regularity ratio of nanopores was registered for the DC mode at 130 V. This can be associated with the thermally enhanced dissolution of oxide as mentioned earlier. It is evident that regularity ratio of nanoporous arrangement and uniformity of nanopores for AC anodized samples are significantly higher than that for DC anodized specimens at similar applied voltages (see Fig. 7 and Table. 1). During AC anodization

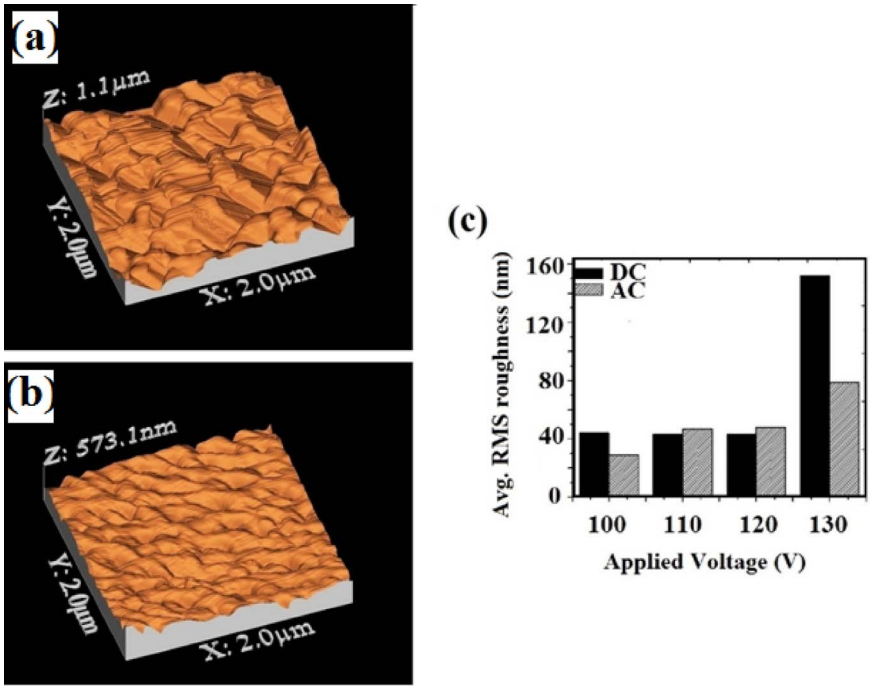


**Fig. 5.** 3D-AFM based surface topographies of anodized samples performed at 130 V. (a) DC mode; (b) AC mode and (c) estimated RMS roughness of anodized samples as a function of applied voltage in DC and AC modes.

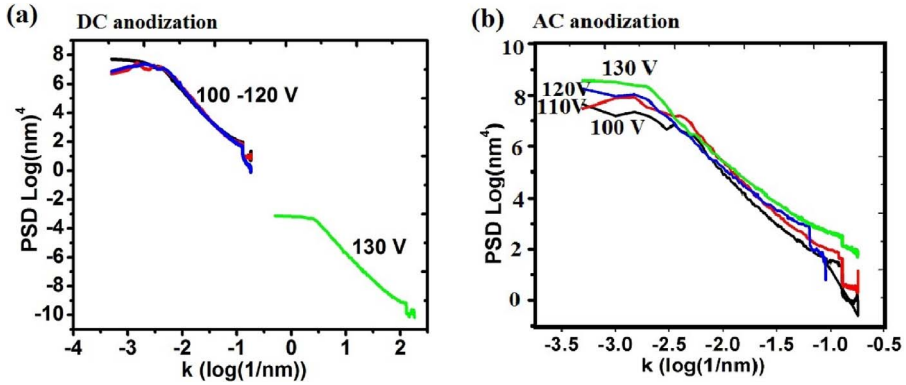


**Fig. 6.** Power spectral density profiles of anodized samples derived from AFM images for (a) DC and (b) AC modes of anodization.

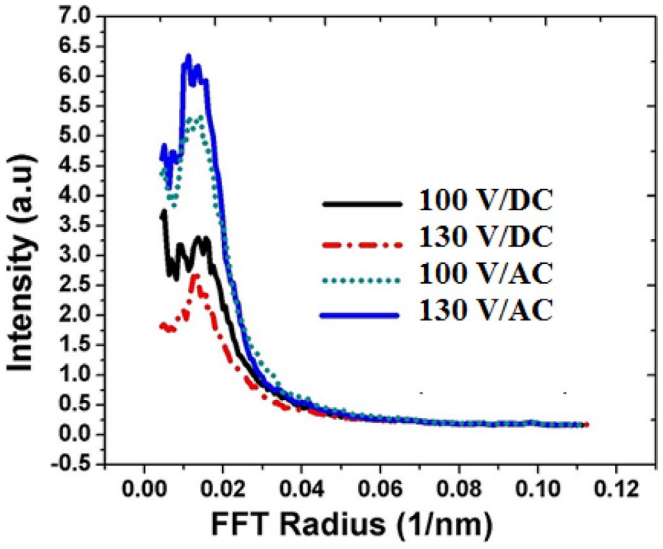


**Fig. 7.** Fast Fourier transforms profiles derived from SEM images for commercial grade aluminum anodized using DC and AC modes.

process, hydrogen/oxygen gases which evolved during the cathodic/anodic cycles are being expected to impose isotropic pressure within the alumina nanopores which eventually tending to produce better regularity ratio of nanoporous arrangement. This hypothesis appears to be consistent with oxygen bubble effect which imparts certain level of isotropic pressure to the cell walls of oxide film and brings some level of ordered nanoporous arrangement [12]. Chu et al [13] observed experimentally that surface morphology of anodizing front can be composed of traces of gas pores after SEM examination. Furthermore, Zaraska et al [14] pointed out that the complete reorganization of nanopores in the phosphoric acid electrolyte can be attributed to the oxygen gas evolution occurring during anodization. In accordance with Pashchanka-Schneider model [16], self-ordering voltage is 160 V for phosphoric acid as mentioned earlier. In the present work, ordering of porous arrangement may enhance with increasing of voltage as voltage difference provides the driving force for pattern formation [16]. For instance, it can be seen that regularity ratio of porous arrangement increases steadily from 2.9 to 4.9 when voltage is increased from 100 to 130 V as mentioned in Table 1. Stepniowski et al [48] also mentioned that greater the applied voltage and temperature, better the regularity ratio of nanoporous arrangement during aluminum anodization. Although debate continues on various existing theoretical models, the evolution of flower-like morphology can be explained successfully by Pashchanka-Schneider model [16]. The trend in the regularity ratio of nanopores for AC anodized specimen appears to be quite consistent with oxygen bubble effect [12]. This means that surface morphology of nanoporous arrangement during AC anodization may be determined by synergism between oxygen bubble effect, and Rayleigh convective cells in accordance with Pashchanka-Schneider model [16].

## 4. Conclusions

1. No significant change in surface morphological features was observed until 120 V irrespective of the polarity or applied voltages. However, DC anodization suffered from filament-like cavities with unusual surface roughness at 130 V. This can be ascribed with thermally enhanced dissolution of oxide at impurity or defect sites.
2. Nanoporous AAO films experienced localized flower-like morphology for all the applied voltages during AC anodization. Evolution of flower-like morphology can be explained successfully by Pashchanka-Schneider model.
3. The regularity ratio of nanoporous arrangement was found to be superior during AC anodization when compared to DC anodization. This could be associated with oxygen bubble effect which brings some level of ordering. This demonstrates that the mechanism of nanoporous pattern formation is primarily controlled by the combination between oxygen bubble effect and Rayleigh convective cells during AC anodization.

## Acknowledgements

The authors would like to express their gratitude for the technical support provided by Mr. Dilbagh Singh, and Mr. Ram Kumar during the entire course of experimentation.

## References

[1] A.M.M. Jani, D. Losic, N.H. Voelcker, Nanoporous anodic aluminum oxide: advances in surface engineering and emerging applications, Prog. Mater. Sci. 58 (2013) 636–704.
[2] W. Yang, C. Cui, Q. Liu, B. Cao, L. Liu, Y. Zhang, Fabrication and magnetic properties of $Sm_2Co_{17}$ and $Sm_2Co_{17}$ /$Fe_7$ $Co_3$ magnetic nanowires via AAO templates, J. Crystal Growth 399 (2014) 1–6.
[3] S.W. Hong, J. Bae, B. Koo, Y.B. Kim, High-performance ultra-thin film solid oxide fuel cell using anodized-aluminum-oxide supporting structure, Electrochem. Comm. 47 (2014) 1–4.
[4] B. Kang, U. Yeo, K. Yoo, Anodized aluminum oxide-based capacitance sensors for the direct detection of DNA hybridization, Biosens. Bioelectron. 25 (2010) 1592–1596.
[5] H. Masuda, K. Fukuda, Ordered metal nanohole arrays made by a two-step replication of honeycomb structures of anodic alumina, Science 268 (1995) 1466–1468.
[6] H. Masuda, F. Hasegawa, S. Ono, Self-ordering of cell arrangement of anodic porous alumina formed in sulfuric acid solution, J. Electrochem. Soc. 144 (1997) L127–L129.
[7] H. Masuda, K. Yada, A. Osaka, Self-ordering of cell configuration of anodic porous alumina with large-size pores in phosphoric acid solution, Jpn. J. Appl. Phys. 37 (1998) L1340–L1342.
[8] J. Oh, C.V. Thompson, The role of electric field in pore formation during aluminum anodization, Electrochem. Acta 56 (2001) 4044–4051.
[9] H. Wu, K.R. Herbert, Electrochemical transients during the initial moments of anodic oxidation of aluminium, Electrochim. Acta 47 (2002) 1373–1383.

[10] G.K. Singh, A.A. Golovin, I.S. Aranson, Formation of self-organized nanoscale porous structures in anodic aluminum oxide, Phy. Rev: B 73 (2006) 2054.
[11] J.E. Houser, K.R. Hebert, The role of viscous flow of oxide in the growth of self-ordered porous anodic alumina films, Nat. Mater 8 (2008) 415–420.
[12] S.J. Garcia-Vergara, P. Skeldon, G.E. Thompson, H. Habazaki, A flow model of porous anodic film growth on aluminium, Electrochim. Acta. 52 (2006) 681–687.
[13] X.F. Zhu, D.D. Li, Y. Song, Y.H. Xiao. The study on oxygen bubbles of anodic alumina based on high purity aluminum, Mater. Lett. 59 (2005) 3160–3163.
[14] L. Zaraska, A. Brudzisz, E. Wierzbicka, G.D. Sulka, The effect of electrolyte change on the morphology and degree of nanopore order of porous alumina formed by two-step anodization, Electro Chemica. Acta 198 (2016) 259–267.
[15] V. Cheim Chu, H. Li, H. Kim, J.M. Seo, Effect of bubble gas on the formation of self-organized pore arrays in anodic aluminium oxide, J. Kor. Phy. Soc. 54 (2009) 2415–2419.
[16] M. Pashchanka, J.J. Schneider, Origin of self-organisation in porous anodic alumina films derived from analogy with Rayleigh–Bénard convection cells, J. Mater. Chem. 21 (2011) 18761.
[17] M. Pashchanka, J.J. Schneider, Self-ordering regimes of porous anodic alumina layers formed in highly diluted oxalic acid electrolyte", Phys. Chem. Chem. Phys. 18 (2016) 6946–6953.
[18] M. Pashchanka, J.J. Schneider, Evidence for electrohydrodynamic convection as a source of spontaneous self-ordering in porous anodic alumina films, Phys. Chem. Chem. Phys. 18 (2016) 6946–6953.
[19] A.M. Abd-Elnaiem, A. Gaber, Parametric Study on the anodization of pure aluminum thin film used in fabricating nano-pores template, Int. J. Electrochem. Sci. 8 (2013) 9741–9751.
[20] W.J. Stępniowskia, A. Nowak-Stępniowskab, A. Preszc, T. Czujkoa, R.A. Varind, The effects of time and temperature on the arrangement of anodic aluminum oxide nanopores, Mater. Character. 91 (2014) 1–9.
[21] S.T. Abrahami, T. Hauffman, J.M.M. de Kok, H. Terryn, J.M.C. Mol, The role of acid-base properties in the interactions across the oxide-primer interface in aero-space applications, Surf. Interface Anal. 48 (2016) 712–720.
[22] W.J. Stępniowski, D. Forbot, M. Norek, M. Michalska-Domańska, A. Król, The impact of viscosity of the electrolyte on the formation of nanoporous anodic aluminum oxide, Electrochim. Acta. 133 (2014) 57–64.
[23] W.J. Stępniowski, M. Moneta, M. Norek, M. Michalska-Domańska, A. Scarpellini, M. Salerno, The influence of electrolyte composition on the growth of nanoporous anodic alumina, Electrochim. Acta. 211 (2016) 453–460.
[24] A.P. Li, F. Muller, A. Birner, K. Nielsch, U. Gosele, Hexagonal pore arrays with a 50–420 nm interpore distance formed by self-organization in anodic alumina, J. Appl. Phys. 84 (11) (1998) 6023–6026.
[25] F. Nasirpouri, M. Abdollahzadeh, M.J. Almasi, N. Parvini-Ahmadi, A comparison between self-ordering of nanopores in aluminum oxide films achieved by two- and three-step anodic oxidation, Curr. Appl. Phys. 9 (2009) S91–S94.
[26] M. Ghorbani, F. Nasirpouri, A. Irajizad, A. Saedi, On the growth sequence of highly ordered nanoporous anodic aluminum oxide, Mater. Design 27 (2006) 983–988.
[27] F. Li, L. Zhang, R.M. Metzger, On the growth of highly ordered pores in anodized aluminum oxide, Chem. Mater. 10 (1998) 2470–2480.
[28] H.J. De Wit, C. Wijenberg, C. Crevecoeur, The dielectric breakdown of Anodic Aluminum Oxide, J. Electrochem. Soc. 123 (1976) 1479–1486.
[29] I. De Graeve, H. Terryn, G.E. Thompson, AC-anodising of aluminium: Contribution to electrical and efficiency study, Electrochem. Acta 52 (2006) 1127–1134.
[30] Li Lingchuan, AC anodization of aluminum, electrodeposition of nickel and optical property examination, Sol. Energy Mater. Sol. Cells 64 (3) (2000) 279–289.
[31] W. Lee, K. Schwirn, M. Steinhart, E. Pippel, R. Scholz, U. Gösele, Structural engineering of nanoporous anodic aluminium oxide by pulse anodization of aluminium, Nat. Nanotechnol. 3 (2008) 234–239.
[32] C.S. Law, A. Santos, M. Nemati, D. Losic, Structural engineering of nanoporous anodic alumina phtonic crystals by sawtooth-like pulse anodization,Appl, Mater. Interf. 8 (2016) 13542–13554.
[33] C.K. Chung, W.T. Chang, M.W. Liao, H.C. Chang, Improvement of pore distribution uniformity of nanoporous anodic aluminum oxide with pulse reverse voltage on low-and-high-purity aluminum foils, Mater. Lett. 88 (2012) 104–107.
[34] CK Chung, RX Zhou, TY Liu, WT Chang, Hybrid pulse anodization for the fabrication of porous anodic alumina films from commercial purity (99%) aluminum at room temperature, Nanotech 20 (2009) 055301.
[35] M. Norek, W.J. Stępniowski, M. Polanski, D. Zasada, Z. Bojar, J. Bystrzycki, A comparative study on the hydrogen absorption of thin films at room temperature deposited on non-porous glass substrate and nano-porous anodic aluminum oxide (AAO) template, Int. J. Hydrogen Energy 36 (2011) 11777–11784.
[36] M. Norek, W.J. Stępniowski, D. Zasada, K. Karczewski, J. Bystrzycki, Z. Bojar, H2 absorption at ambient conditions by anodized aluminum oxide (AAO) pattern-transferred Pd nanotubes occluded by Mg nanoparticles, Mater. Chem. Phys. 133 (2012) 376–382.
[37] A. Brzózka, D. Szeliga, E. Kurowska-Tabor, G.D. Sulka, Synthesis of copper nanocone array electrodes and its electrocatalytic properties toward hydrogen peroxide reduction, Mater. Lett. 174 (2016) 66–70.
[38] A. Brzózka, A. Jeleń, A.M. Brudzisz, M.M. Marzec, G.D. Sulka, Electrocatalytic reduction of chloroform at nanostructured silver electrodes, Electrochim. Acta. 225 (2017) 574–583.
[39] E. Kurowska, A. Brzózka, M. Jarosz, G.D. Sulka, M. Jaskuła, Silver nanowire array sensor for sensitive and rapid detection of H2O2, Electrochim. Acta. 104 (2013) 439–447.
[40] T. Masuda, H. Asoh, S. Haraguchi, S. Ono, Nanoporous alpha;-alumina membrane prepared by anodizing and heat treatment, Electrochemistry 82 (2014) 448–455.
[41] T. Masuda, H. Asoh, S. Haraguchi, S. Ono, Fabrication and characterization of single phase α-alumina membranes with tunable pore diameters, Materials 8 (2015) 1350–1368 (Basel).
[42] M.A. van Put, S.T. Abrahami, O. Elisseeva, J.M.M. de Kok, J.M.C. Mol, H. Terryn, Potentiodynamic anodizing of aluminum alloys in Cr(VI)-free electrolytes, Surf. Interface Anal. 48 (2016) 946–952.
[43] S.T. Abrahami, T. Hauffman, J.M.M. De Kok, J.M.C. Mol, H. Terryn, XPS analysis of the surface chemistry and interfacial bonding of barrier-type Cr(VI)-free anodic oxides, J. Phys. Chem. C. 119 (2015) 19967–19975.
[44] F. Keller, M.S. Huntey, D.L. Robinson, Structural features of oxide coatings on aluminium, J. Electrochem. Soc. 100 (1953) 411–419.
[45] M.K. Kushwaha, S. Anjan, S. Ray, Carbon nanotube/nanofiber embedded nano-porous anodized aluminium oxide surface and its tribological properties, J. Nanosci. Nanotech. 8 (2008) 4152–4157.
[46] J.P. Tu, C.X. Jiang, S.Y. Guoc, X.B. Zhaoa, M.F. Fu, Tribological properties of aligned film of amorphous carbon nanorods on AAO membrane in different environments, Wear 259 (2005) 759–764.
[47] C.J. Buchko, K.M. Kozloff, D.C. Martin, Surface characterization of porous, biocompatible protein polymer thin films, Biomaterials 22 (2001) 1289–1300.
[48] W.J. Stępniowski, M. Michalska-Domańska, M. Norek, T. Czujko. Fast Fourier transform based arrangement analysis of poorly organized alumina nanopores formed via self-organized anodization in chromic acid. Mater. Lett. 117(2014) 69–73.
[49] Horcas,R. Fernández, J.M. Gómez-Rodríguez, J. Colchero, J. Gómez-Herrero, A.M. Baro, WSXM: a software for scanning probe microscopy and a tool for nanotechnology, Rev. Sci. Instrum. 78 (2007) 013705.
[50] WSxM, http://www.nanotec.es (Last Accessed.